Talanta 221 (2021) 121372

Contents lists available at ScienceDirect

Talanta

journal homepage: www.elsevier.com/locate/talanta

Synthesis of highly fluorescent carbon dots as a dual-excitation rationmetric fluorescent probe for the fast detection of chlorogenic acid

Qingshi Liu [a], Zhichen Dong [a], Aijun Hao [b], Xingjia Guo [a,*], Wei Dong [c,**]

[a] College of Chemistry, Liaoning University, Shenyang, 110036, China
[b] College of Pharmacy, Liaoning University, Shenyang, 110036, PR China
[c] Department of Chemistry, Shenyang Medical College, Shenyang, 110036, China

ARTICLE INFO

Keywords:
Fluorescent carbon dots
Chlorogenic acid
Rationmetric fluorescent probe
Inner filter effect

ABSTRACT

Nitrogen and sulfur co-doped carbon dots (abbreviated as N,S-CDs) were obtained by two-step hydrothermal reactions using citric acid/sulfamic acid as precursors, polyethyleneimine (PEI) as passivation agent. It was found that the PEI modified CDs with a fluorescence quantum yield of up to 29.1%, showed an obviously enhanced photoluminescence (PL) compared to the initial CDs. Interestingly, when monitored at the fluorescence emission wavelength of 460 nm, the dispersed N,S-CDs solution exhibits only one excitation band peaked at 355 nm, while one aggregated N,S-CDs solution with good water solubility and excellent fluorescence stability possesses two well-separated excitation bands centered at 310 nm/397 nm. When chlorogenic acid (CGA) was added to this aggregated N,S-CDs solution, the excitation peak at 310 nm was obviously reduced due to the inner filter effect (IFE), whereas another peak at 397 nm almost remained constant. Based on the above phenomenon, a dual-excitation ratiometric fluorescent probe for CGA assay was constructed. Under the optimized conditions, the logarithm of the fluorescence intensity ratios (F_{397}/F_{310}) exhibited a good linear correlation with the CGA concentration over a range from 0.33 to 29.70 μg/mL with a detection limit of 0.12 μg/mL. Moreover, the proposed sensing system was applied to determine CGA content in real samples with satisfactory results. The proposed sensing platform provides a new method for the detection of CGA.

1. Introduction

So-called carbon dots are considered to be one type of fluorescent nanomaterials with sizes generally below 10 nm, exhibiting unique luminescent properties due to the quantum confinement and edge effects. Since the first discovery by Xu in 2004 [1], they have drawn increasing attention in aspects of synthesis and application. Because carbon quantum dots have good optical properties, excellent water solubility, low toxicity, environmental friendliness, wide range of raw materials, low cost, good biocompatibility, etc., they have been applied in many aspects, such as medical imaging technology, light-emitting diodes, chemical and biological sensors [2–5]. Compared with organic dyes and metal-containing quantum dots, the carbon quantum dots pose great potential application prospects in many fields.

In the past decade, a variety of methods for synthesizing carbon dots have been developed. These methods can be roughly divided into two classes, namely top-down fabrication and bottom-up synthesis according to different carbon sources [6]. To date, the synthesis techniques of carbon dots mainly include hydrothermal or solvothermal method, electrochemical, microwave-assisted or ultrasonic process, and so on. Hydrothermal synthesis refers to heterogeneous reactions in aqueous media under high temperature and pressure. The reaction process is simple and easy to control the size, composition and purity, so it is more commonly adopted for the synthesis of CDs [7,8]. In order to improve the chemical and luminescent properties of carbon dots, the chemical structures related to their core and surface need to be appropriately modulated. Heteroatomic doping and surface modification have proved to be effective strategies of turning CDs [9,10]. Usually, nitrogen, phosphorus, boron and sulfur are often doped into CDs [9–11]. For instance, Ding et al. successfully synthesized strong blue emitting N,S co-doped carbon dots via the hydrothermal treatment and they thought the obviously improved PL efficiency should be ascribed to the synergistic effect of nitrogen and sulfur doping [12]. The surface modification is also an efficient route to further enhance the luminescence efficiency

* Corresponding author.
** Corresponding author.
E-mail addresses: guoxja@sina.com (X. Guo), dongwei5873@126.com (W. Dong).

https://doi.org/10.1016/j.talanta.2020.121372
Received 25 December 2019; Received in revised form 29 June 2020; Accepted 30 June 2020
Available online 6 September 2020
0039-9140/

of CDs [13]. Polymers have been widely employed to modify the surface of CDs [14]. For example, CDs passivated with PEI could improve their fluorescence intensity owing to the successful introduction of nitrogen-containing groups onto their surfaces [15].

Chlorogenic acid, which is high in various medicinal plants, such as honeysuckle and eucommia, is a kind of phenylpropanoid compound produced by plants during aerobic respiration and has a wide range of biological activities [16]. CGA has antibacterial, antiviral, anti-oxidation effects, and can increase white blood cells, liver and gallbladder, anti-tumor, blood pressure lowering blood lipids, scavenging free radicals and exciting central nervous system [17–19].

The analytical methods of CGA mainly include high performance liquid chromatography [20], liquid chromatography-mass spectrometry [21,22] and thin-layer scanning [23]. However, these methods are expensive, the sample preparation is complicated, the measurement time is too long, and the efficiency is low, so they have certain limitations. Thus, it is necessary to develop an efficient, simple, fast, low-cost and eco-friendly method for the detection of CGA.

Single emission fluorescent sensors have proven to be an effective tool compared to other detection techniques due to their many advantages, including simple operation, high sensitivity and selectivity. For example, Wang et al. synthesized water-soluble CdTe quantum dots for the detection of CGA [24]; Yang et al. [25] synthesized the fluorescent carbon dots using malic acid and urea as precursors, and established a quantitative detection method towards CGA based on the IFE. However, these methods based on single-emission signal are easily disturbed by some variable factors, such as light-source intensity and environmental conditions [26]. The ratiometric fluorescence method can just overcome these drawbacks because of the advantages of dual emission. Consequently, ratiometric fluorescence sensors have received increasing interest recently [27–29]. In ratiometric fluorescent probes related to fluorescent carbon dots, two fluorescence signals are simultaneously measured at different wavelengths and their intensity ratio is then used to quantitative analysis. Usually, these two fluorescent signals originate from CDs and other fluorescent nanoparticles or fluorescent dyes [29,30]. Thus, the construction of ratiometric fluorescent probe often involves in tedious multistep preparation and sophisticated coupling or chemical modification process [31]. Herein, we simplified the construction process and only utilized one kind of CDs to design a novel dual-excitation ratiometric fluorescence probe for detection of CGA.

In this work, we successfully fabricated nitrogen and sulfur co-doped strong blue-emitting carbon dots via two-step hydrothermal process. After the detailed characterizations, the aggregated N,S-CDs serve as an IFE-based ratiometric fluorescent probe for the quantitative determination of CGA. The fluorescent signals at excitation wavelengths of 310 nm and 397 nm were recorded for calculating fluorescence ratios. Then, the proposed sensor was applied to detect real samples for evaluating its analysis performance.

2. Experimental

2.1. Chemicals and reagents

All chemicals used in this experiment were not further purified. Citric acid was acquired from Tianjin Damao Chemical Reagent Factory (China). Sulfamic acid was obtained from Shandong Xinda Chemical Co., Ltd. (China). Quinine sulfate was obtained from Jinan Oumi Biological Technology Co., Ltd. (China). Chlorogenic acid (CGA) was purchased from Shanghai Maclean Biochemical Technology Co., Ltd. (China). Polyethyleneimine (PEI) (branched, M.W. 600, 99%) was obtained from Shandong Xiya Chemical Co., Ltd. (China). All other reagents used in this study were of analytical grade or above and obtained from Sinopharm Chemical Reagent Co., Ltd (China). Double distilled water was used through the experiment. Citric acid/sodium citrate buffer solution (pH 4.0) was used to control the acidity of the aqueous solutions.

2.2. Synthesis of N,S-CDs

Typically, 0.25 g of sulfamic acid and 1.0 g of citric acid were mixed thoroughly, then the resulting mixture was transferred into a 50 mL Teflon-lined stainless autoclave. Next, the autoclave was heated in a drying oven at 190 °C for 5 h after the reaction, the above autoclave was naturally cooled to room temperature. Larger particles in the obtained product was removed by centrifugation at 10000 rpm for 10 min. Then 0.25 g of PEI and 20 mL of distilled water were added into the above initial CDs solution. Once completely mixing, the above mixture in the autoclave was heated in a drying oven at 160 °C for 12 h, finally a deep brownish yellow liquid was obtained. After that, the liquid was filtered with a 0.22 μm filter, and then centrifuged at 10000 rpm for 10 min. The obtained supernatant was dialyzed against water using a dialysis bag with a molecular weight cut off = 1000 Da for 48 h to remove residual reagents. Finally, the purified solution (noted as solution O) was freeze-dried to obtain the brown solid powder or diluted for preparing some working solutions.

2.3. Characterization of the synthesized N,S-CDs

The morphologies and the size of the N,S-CDs was characterized using a JEM-2100 transmission electron microscope (TEM) (JEOL Ltd., Japan) at an acceleration voltage of 100 kV. A drop of aqueous sample was dispersed on a carbon-coated copper grid and dried at room condition for TEM observation. X-ray diffraction (XRD) patterns were obtained on an X-ray diffractometer (Bruker-Axs, Karlsruhe, Germany) using Cu Kα radiation (λ = 0.1546 nm). Fourier transform infrared (FTIR) spectra were recorded on a Nicolet Avatar 330 FT-IR spectrometer (Thermo Electron Corporation, USA) with a KBr pellet. The X-ray photoelectron spectrum (XPS) was recorded using an ESCALAB 250Xi spectrometer (Thermo Fisher). UV–vis absorption spectra were recorded via a TU-1800PC UV–vis spectrophotometer (Varian Company, USA), while fluorescence measurements were performed on a Cary Eclipse 300 FL spectrophotometer (Varian Company, USA) equipped with a 1.0 cm quartz cell. Cyclic voltammetry curves of N,S-CDs were measured using a CHI660D electrochemical workstation with a three-electrode system (Shanghai Chenhua Apparatus Corporation, China). Firstly, the glassy carbon electrode (GCE) was polished, washed and dried in exactly the same manner as described in the literature [32], and then, 100 μL of the N,S-CDs was mixed with 100 μL Nafion (0.5 wt%). Afterwards, the obtained mixture was added on the surface of the GCE using a microsyringe, finally air dried for use. Zetasizer Nano-ZS 90 analyzer (Malvern, U.K.) was used to measure the zeta potential of N,S-CDs. All the measurements were performed at room temperature if not specified otherwise.

2.4. Procedure of CGA detection

The excitation spectra of a series of different fold dilution of solution O (pH 4.0) were scanned at a fixed fluorescence emission wavelength of 460 nm. When two well separated and strong fluorescence excitation peaks were observed, the corresponding aggregated N,S-CDs solution (denoted as solution A) was used to construct a dual-excitation ratiometric fluorescent probe for the detection of CGA. All fluorescence measurements were conducted for three times in the consequent experiment.

A series of different volumes of CGA stock solution (0.5 mg/mL) were added to a quartz cuvette containing a 3 mL of solution A (pH 4.0) one by one using a microinjector. After each sample was incubated for 5 min, the two excitation spectra were recorded at the fluorescence emission wavelength of 460 nm. The excitation/emission slit width was adjusted at 5 nm. A pH 4.0 citric acid/sodium citrate buffer solution was used to control the pH and all of these experiments were carried out at room temperature.

For the selectivity test toward CGA, some metal ions, anion ions and

organic molecules as potential interfering substances were chosen to instead of CGA under the same conditions.

For real sample analysis, shuanghuanglian oral liquid samples were purchased from a local pharmacy store and filtered through a 0.22 μm polystyrene filter and the human blood serum samples were obtained from healthy volunteers at the local hospital. After adding acetonitrile to the serum sample, the mixture was centrifuged for 10 min at 10000 rpm to obtain protein-free serum samples. All the samples were stored at 4 °C prior to use. Each treated sample was spiked with different volumes of CGA stock solution (final concentration: 3.33, 6.67 and 9.99 μg/mL) and the spiked sample solutions were analyzed with the above described process.

2.5. Quantum yield measurements

The fluorescence quantum yield (QY) of N,S-CDs was determined by comparative method using quinine sulfate (QY = 54%) in 0.1 M H_2SO_4 as reference [32]. The absorptions of the sample and the standard solutions at 355 nm were respectively measured (less than 0.1), and their fluorescence emission spectra were scanned. Finally, the quantum yield was estimated as follows:

$$Y_c = Y_r \frac{I_c A_r n_c^2}{I_r A_c n_r^2} \quad (1)$$

where Y is the quantum yield, and n the refractive index of the solvent (1.33). A is the absorbance, and I the peak area of the fluorescent peak. Subscripts r and c represent the standard and the sample, respectively.

3. Results and discussion

3.1. Characterization of N,S-CDs

Fig. 1 is the TEM image and particle size distribution image of the as-prepared N,S-CDs. It was found that uniformly dispersed CDs with an average diameter of about 5.1 nm are spherical shape and their sizes range from 3.0 to 8.0 nm. That larger particles were observed should be attributed to the surface passivation by PEI.

In order to further identify the crystalline nature of the N,S-CDs, the XRD pattern was recorded. As depicted in Fig. 2A, one broad peak near $2\theta = 22.5°$ was observed, disclosing an amorphous carbon phase caused by the introduction of nitrogen- and oxygen-containing groups [33].

Fourier Transform Infrared (FTIR) spectroscopy is often used to identify the surface groups of nanoparticles. The FTIR spectrum of the N,S-CDs was recorded as shown in Fig. 2B. One broad and strong peak around 3427 cm^{-1} is attributed to the stretching vibration peak of N–H/O–H [15]. The peaks around 1700 and 1600 cm^{-1} belong to the stretching vibrations of C═O in the COOH and $CONH_2$ groups, respectively [34]. The in-plane bending vibration of N–H and the stretching vibration peak of C–N both appear at 1380 cm^{-1}; the peaks at 1138 and 1097 cm^{-1} are assigned to the stretching vibrations of C–O and $-SO_3^-$, respectively [35]. The above results demonstrate the existence of hydroxyl, carboxy and amine groups on the surface of N,S-CDs and these hydrophilic groups enhance solubility.

For exploring the elemental composition and chemical bonds, XPS spectra of N,S-CDs were recorded and presented in Fig. 3. The XPS survey spectrum in Fig. 3A reveals that N,S-CDs are mainly composed of C, N, O, S elements, the corresponding contents were 65.24%, 11.55%, 22.11% and 1.10%, respectively. The high resolution XPS spectrum of C1s (Fig. 3B) [36] displays three peaks with binding energy at 284.8 eV, 286.0 eV and 288.1 eV. These peaks are assigned to C–C, C–N/C–O and C═O bonds, respectively. As can be seen from the N1s spectrum (Fig. 3C) [37], there are two distinct peaks at 399.6 eV and 401.0 eV, corresponding to N–C, and N–H, respectively. The O1s spectrum (Fig. 3D) [38] contains three peaks at 531.2 eV and 532.4 eV, indicating the existing forms of O on N,S-CDs, namely C–OH/C–O–C, C═O. The S2p spectrum (Fig. 2E) [37] shows the presence of C-SO_x (x = 2–4) species of which binding energies are between 168.0 and 169.1 eV. The results of XPS further reconfirm the above FTIR analysis.

3.2. Optical properties of N,S-CDs and optimization of analytical parameters

Fig. 4A depicts the PL spectra of the dispersed N,S-CDs solution at different excitation wavelengths ranging from 300 to 450 nm in a 10 nm increments. The maximum emission wavelength was found to be red-shifted by about 44 nm, indicating that the synthesized N,S-CDs also exhibit excitation-dependence behavior, which should originate from the effects of particles sizes and different distribution of emissive energy traps on the surface of CDs [15,39]. The fluorescence quantum yield of N,S-CDs was calculated to be 29.1% using quinine sulfate as a standard. In this experiment, we found that the carbon dots obtained in the first step synthesis emitted quite weak blue fluorescence under UV light radiation. So an obvious enhancement in the fluorescence efficiency of N,S-CDs should be attributed to the effective passivation effect of PEI on the surface defects.

As for the obtained N,S-CDs, we found an interesting phenomenon: when the fluorescence emission wavelength of 460 nm was fixed for scanning the excitation spectrum of one aggregated N,S-CDs solution, there were two distinct fluorescence excitation peaks (curves a and b shown in Fig. 4B). Moreover, as the aggregated N,S-CDs solution was diluted, these two excitation peaks approached each other until they overlapped one peak centered at 355 nm as shown in Fig. S1, meanwhile, the corresponding fluorescence intensities gradually increased. These results also demonstrate that the carbon dots with different degrees of aggregation possess the similar distribution of emitting centers on their surfaces, just like molecular fluorescence, no matter which higher level state one molecule is excited to, it will emit fluorescence

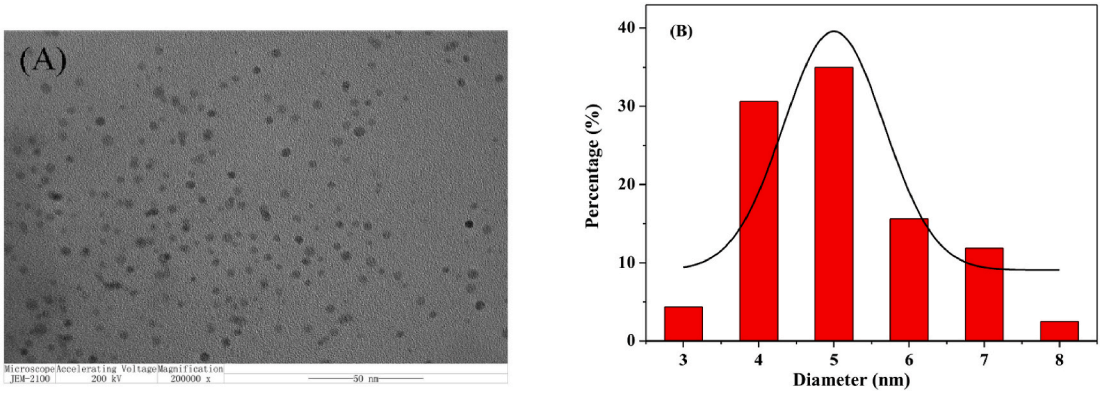

Fig. 1. TEM image (A) and the size distribution histogram (B) of the as-prepared N,S-CDs.

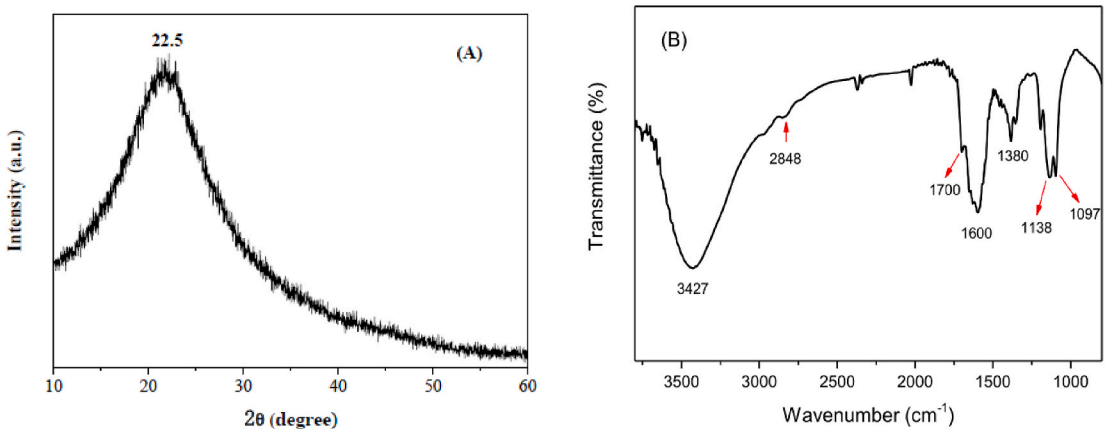

Fig. 2. XRD pattern (A) and FTIR spectrum (B) of the N,S-CDs.

through one transition from the lowest energy level of the first excited state to one energy level of the ground state. Thus, different dilution multiples of solution O have the same emission maximum wavelength (460 nm). As for the reason why there exist two different excitation peaks for the aggregated N,S-CDs solutions, we think that the aggregated N,S-CDs possess two different HOMO-LUMO band gaps and the positions of these HOMO and LUMO levels vary with the aggregation degrees of N, S-CDs.

After a series experiments with different dilutions of solution O, as shown in Fig. 6A, it was found that the 100-fold diluted solution (denoted as A) could produce two well-separated and strong excitation bands peaked at 310 nm and 397 nm, respectively. Therefore, solution A was chosen to construct a ratiometric fluorescent probe and the fluorescent intensity at each excitation wavelength was recorded for calculating fluorescence ratio (F_{397}/F_{310}). This sensing strategy is completely different from the previously reported [1–3].

As shown in Fig. 4B, CGA has a characteristic absorption peak which effectively overlaps with the excitation peak at 310 nm of solution A. Thus, an IFE may occur between CGA and solution A. When CGA was added into solution A, the excitation peak at 310 nm was obviously decreased, while another excitation peak (curve b) kept unchanged. Therefore, the proposed ratiometric fluorescent sensor was applied for the detection of CGA.

In order to gain better performance of the sensor, the experimental parameters that are likely to affect detection of CGA including pH value and incubation time were optimized.

Acidity is closely related to the luminescence efficiency of N,S-CDs and also considered as an important factor of affecting detection sensitivity. The effect of acidity on fluorescence intensity ratio (F_{397}/F_{310}) of the solution A containing CGA was investigated by varying pH from 3.0 to 8.0. As depicted in Fig. 5A, the F_{397}/F_{310} at first increased with increasing pH and then decreased. Obviously, the F_{397}/F_{310} value reached a maximum at pH 4.0, so pH 4.0 (citric acid/sodium citrate buffer solution) was chosen as the optimum pH for the sensing system.

Next, the impact of reaction time on F_{397}/F_{310} was explored. As illustrated in Fig. 5B, as adding CGA into solution A (pH 4.0), the F_{397}/F_{310} value slightly fluctuated within 5 min, and after 5 min, the F_{397}/F_{310} remained stable. Therefore, when CGA was added to solution A, in order to ensure an adequate interaction between the target and the carbon dots, the excitation spectra of the mixture were recorded after incubation for 5 min.

Finally, the fluorescence stability of solution A was also examined. Solution A was prepared by diluting solution O with citric acid/sodium citrate buffer solution and then transferred to a quartz cuvette. After the surface of the above cuvette was sealed with thin membrane, the excitation spectra were recorded by fixing the fluorescence emission wavelength at 460 nm every 30 min at room temperature. As shown in Fig. 6B, the two fluorescence excitation peaks did not change significantly as time went on from 0 to 5 h, indicating that solution A shows a good fluorescence stability and has the potential to be applied to construct a fluorescence detection system. As depicted in Scheme 1A, there are many branched chains of PEI on the surfaces of PEI modified nanoparticles, the aggregation of N,S-CDs should mainly depend on hydrogen bonds and the physical intertwining among these chains, resulting in forming more stable the aggregated nanoparticles. Additionally, The zeta potential of N,S-CDs was measured to be nearly zero at pH4.0, which is also beneficial to the aggregation of N,S-CDs.

3.3. Analytical performance of the sensing method

Under the optimized conditions described above, the fluorescence excitation spectra of solution A in the presence of different concentrations of CGA were recorded, respectively. As presented in Fig. 7A, the excitation peak at 310 nm deceased with the gradual increase of CGA concentration, whereas the excitation peak at 397 nm remained nearly constant. The blue plot in Fig. 7B depicts the change of the fluorescence intensity ratio with different concentrations of CG, obviously it cannot be well described by a linear regression curve. Here, the logarithm value of fluorescence intensity ratio displays a good linear relationship with the CGA concentration ranging from 0.33 to 29.70 μg/mL (black plot in Fig. 7B). The linear regression equation is $\lg(F_{397}/F_{310}) = 0.02804 \times [CGA] - 0.1302$ with a correlation coefficient of $R^2 = 0.9970$, which was used to detect CGA. Here, F_{397}/F_{310} is the fluorescence intensity ratios after adding CGA and [CGA] is the concentration of CGA. According to the formula $3S_d/S$, the detection limit of the method was calculated to be 0.12 μg/mL using the above equation, where S_d is the standard deviation of blank signal (n = 11) and S is the slope of the calibration curve. The precision was obtained by measuring 6.67 μg/mL of CGA solution under the optimized conditions. The average result for 5 replicates was calculated to be 6.86 μg/mL with a relative standard deviation of 0.42%. In addition, some previously reported methods for CGA detection are also summarized in Table 1. Compared to the other methods, the proposed assay has not only a wider linear range, but also the lowest detection limit. Meanwhile, it is also a simple, fast, convenient and low-cost method.

3.4. Selectivity for CGA detection

Excellent selectivity is quite important for any kind of fluorescence sensor. Herein, the influences of other coexisting substances on this method were explored. A series of interference experiments were performed by adding appropriate amount of coexisting substances to the solution A containing 6.67 μg/mL of CGA under the optimized conditions. The interfering substances used include: Na^+, Cl^- and K^+ (2.0 ×

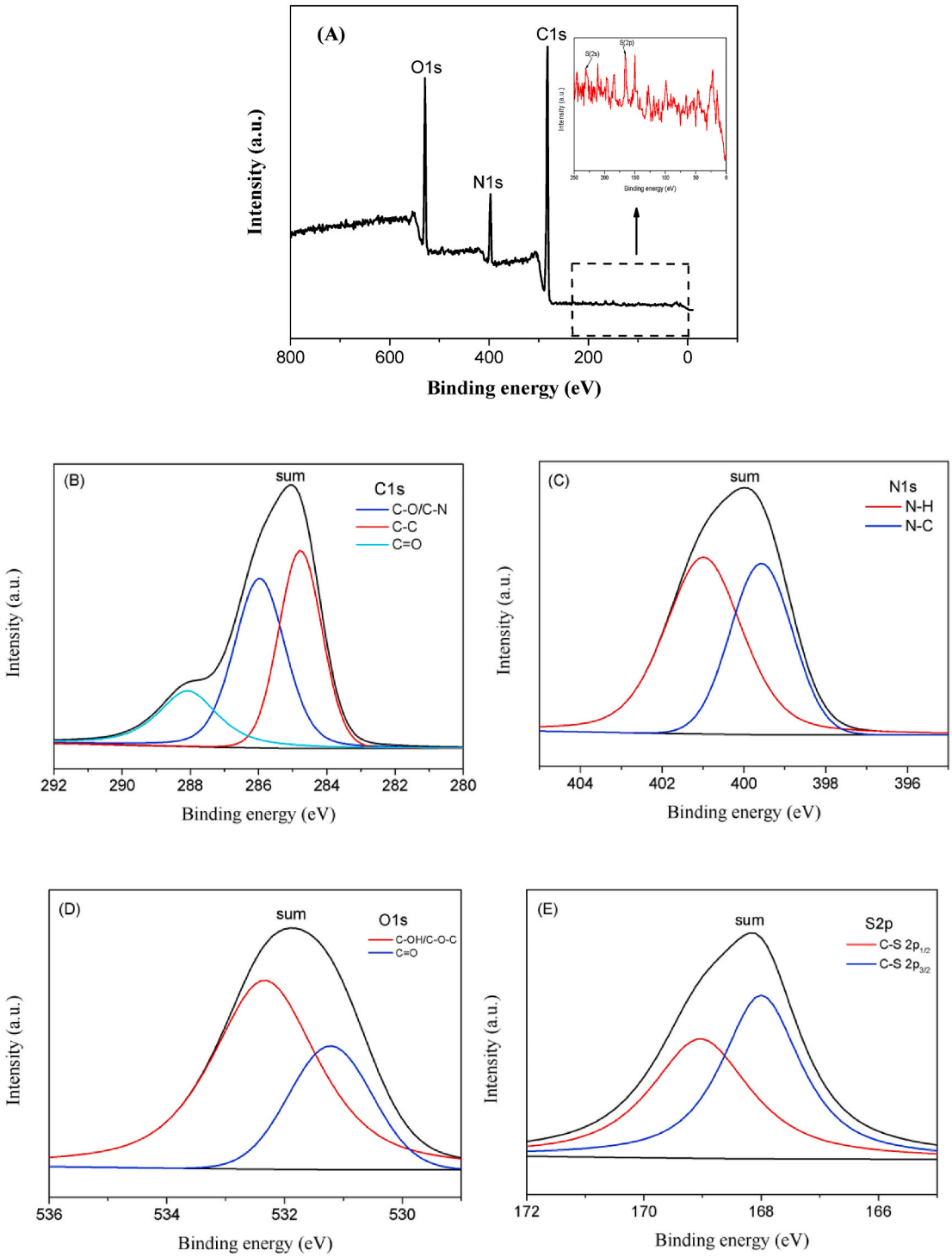

Fig. 3. XPS survey spectrum of the N,S-CDs (A) and XPS high resolution C1s (B), N1s (C), O1s (D) and S2p (E) spectra of the N,S-CDs.

10^{-2} mol/L), Ca^{2+}, Mg^{2+}, Ni^{2+}, Zn^{2+}, Pb^{2+}, Cu^{2+}, Hg^{2+}, Cd^{2+} and Fe^{3+} (3.3×10^{-3} mg/mL), CO_3^{2-}, HCO^{3-}, SO_4^{2+} and NO^{3-} (0.67×10^{-3} mol/L), glycine, urea, glucose, quinic acid and caffeine (0.33×10^{-3} mol/L). The abscissa of Fig. 8 shows the ratio of the F_{397}/F_{310} values of the solution A + CGA mixture in the presence and absence of interfering substance. Except for Fe^{3+}, the other interfering substances showed negligible influences on the detection of CGA. These results demonstrate that the aggregated N,S-CDs based fluorescence sensor was highly selective for detecting CGA in samples containing these potentially interfering substances.

Fe^{3+} can cause obvious fluorescence ratio change of solution A , so its presence will interfere the quantitative determination of CGA in real samples. In this study, the triethanolamine (TEA) solution was chosen to mask Fe^{3+}. As presented Fig. S2, the two excitation peaks of solution A containing Fe^{3+} were effectively recovered after adding TEA. Therefore, TEA can be used to eliminate the interference of Fe^{3+} on the detection of CGA.

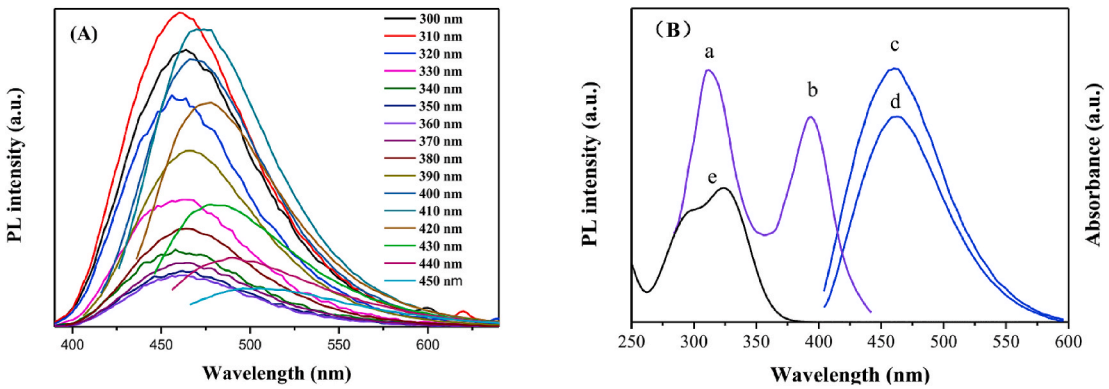

Fig. 4. (A) Fluorescence emission spectra of the dispersed N,S-CDs aqueous solution excited with different wavelengths ranging from 300 to 450 nm in 10 increments. (B) The excitation (a and b) and emission (c and d) spectra of solution A and the absorption spectrum of CGA (e).

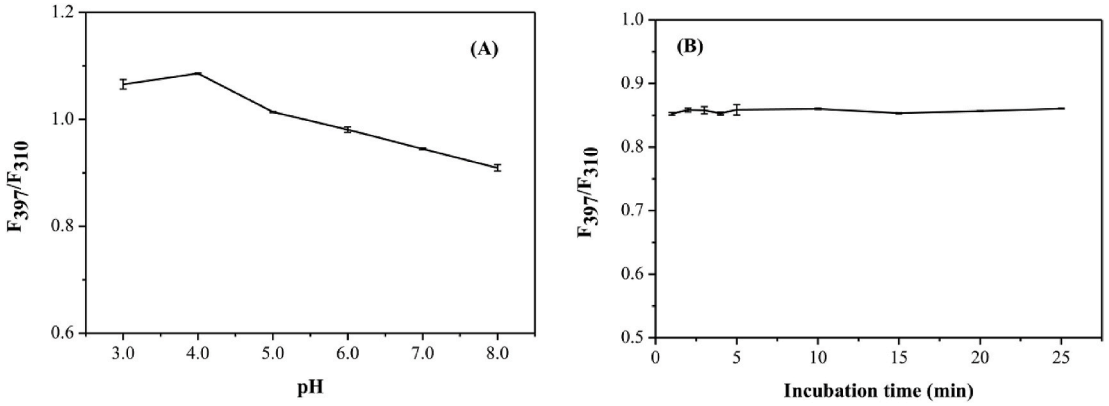

Fig. 5. The effects of pH (A) and incubation time (B) on the fluorescence intensity ratio of solution A.

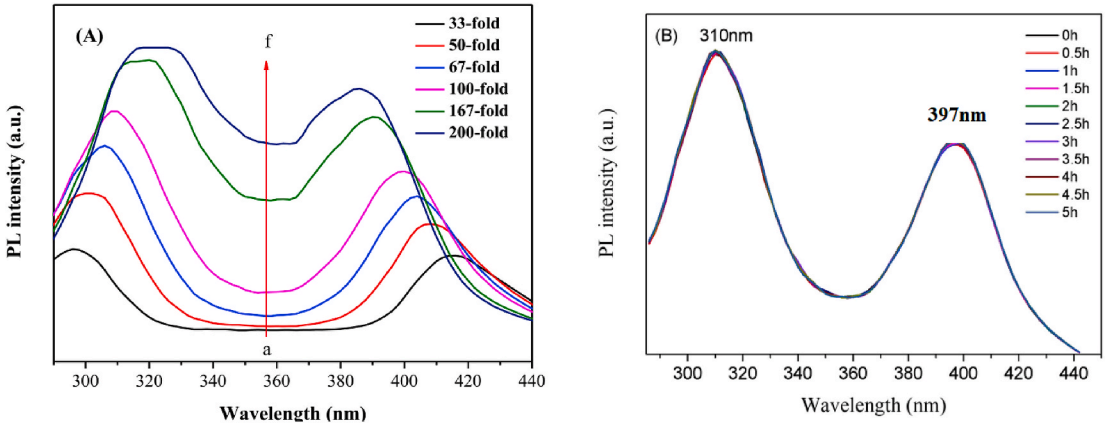

Fig. 6. Fluorescence excitation spectra of different dilution multiples of solution O (from a to f is 33 to 200-fold) (A) and fluorescence excitation spectra of solution A were recorded under the emission wavelength of 460 nm every 30 min of interval at room temperature (B).

3.5. Detection mechanism of probe

Fig. 7A demonstrates that the fluorescence of solution A can be effectively quenched by CGA. Usually the decrease of the donor fluorescence might be related to the energy transfer, IFE and electron transfer [44]. As shown in Fig. 4B, an effective spectral overlap between the excitation band (curve a) of the solution A and the absorption band (curve e) of CGA was observed, indicating that the IFE induced the fluorescence decline of N,S-CDs. In addition, no spectral overlap between the fluorescence emission band of N,S-CDs and the absorption band of CGA was found in Fig. 4B, demonstrating that no energy transfer occurred from N,S-CDs to CGA.

In order to estimate the highest occupied molecular orbital (HOMO) and lowest unoccupied molecular orbital (LUMO) energy levels of the as-prepared N,S-CDs, a cyclic voltammetry (CV) analysis was conducted using a conventional standard three-electrode system, which consists of N,S-CDs modified glassy carbon working electrode, a Pt-wire counter electrode and an Ag/AgCl reference electrode [32]. ECL signals of the N, S-CDs were recorded in 0.1 M KCl solution as the supporting electrolyte. As shown in Fig. 9A, the reduction potential for N,S-CDs is determined to

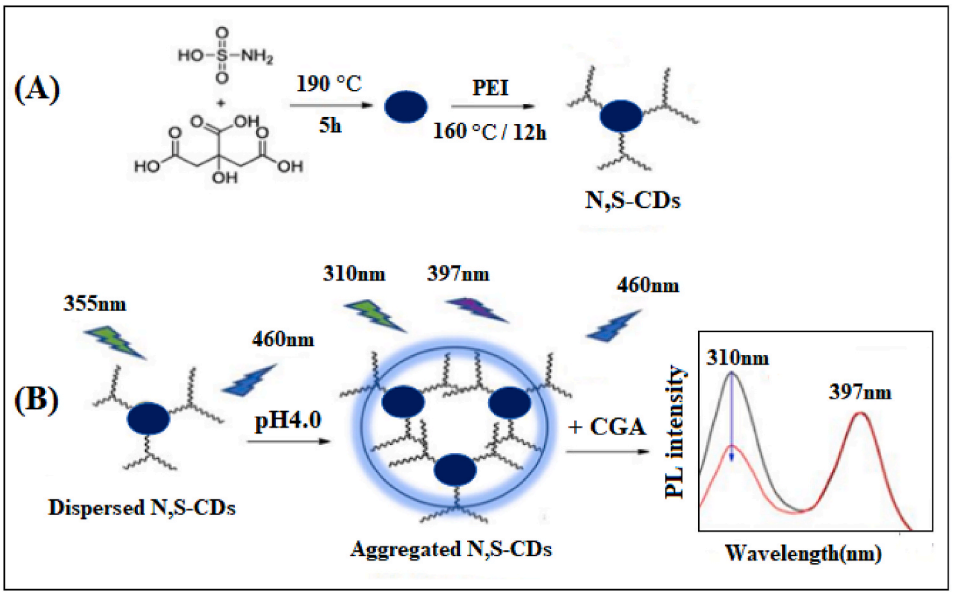

Scheme 1. Schematic illustration of the N,S-CDs synthesis (A) and CGA sensing process (B).

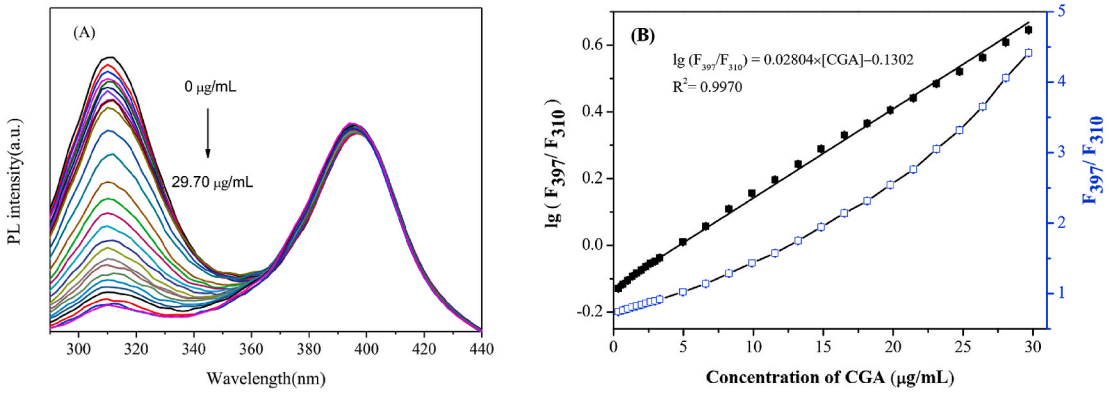

Fig. 7. (A) Fluorescence excitation spectra of solution A after adding different concentrations of CGA (from top to bottom: 0, 0.33, 0.67, 1.00, 1.33, 1.65, 1.98, 2.31, 2.64, 2.97, 3.30, 4.95, 6.60, 8.25, 9.90, 11.55, 13.20, 14.85, 16.5, 18.15, 19.80, 21.45, 23.10, 24.75, 26.40, 28.05, and 29.70 μg/mL) (pH4.0). (B) Plot (blue line) of F_{397}/F310 versus CGA concentration from 0.33 to 29.70 μg/mL and the calibration curve (black line) for CGA detection. (For interpretation of the references to colour in this figure legend, the reader is referred to the Web version of this article.)

Table 1
Comparison of the proposed method with previously reported methods for determining CGA.

Method	Linear range (μg/mL)	LOD (μg/mL)	Ref.
HPLC	10–100	0.26	[40]
Photosensor	5.64–564.48	1.52	[41]
Flow-through chronopotentiometry (FTCP)	14.11–28.22	1.61	[42]
Magnetic dispersive micro-solid phase extraction	114–202	34	[43]
Ratiometric fluorescence probe based N,S-CDs	0.33–29.70	0.12	This work

be −0.63 V vs Ag/AgCl (−0.84 V vs NHE). The HOMO and LUMO energy levels of N,S-CDs can be calculated according to the following equations:

$$E_{LUMO} = -eE_{red} - 4.5eV = -e(-0.84V) - 4.5eV \quad (2)$$

$$= -3.16\ eV$$

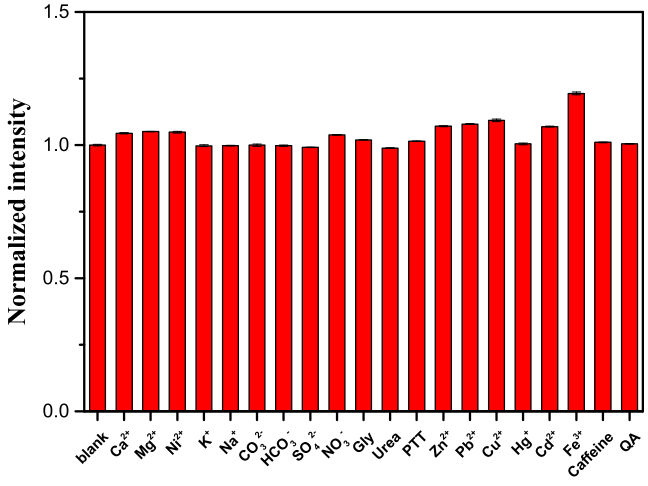

Fig. 8. Effects of potential interfering substances on the detection of CGA.

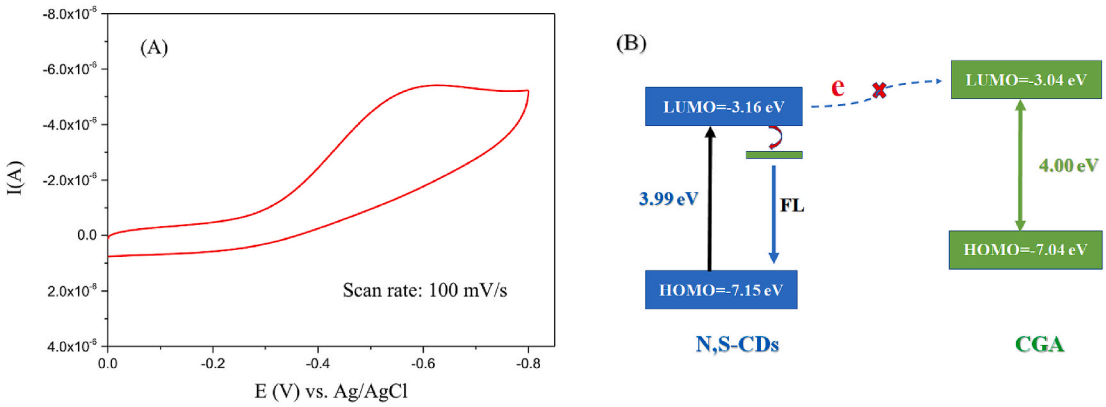

Fig. 9. (A) Cyclic voltammetry curves of N,S-CDs on the GCE. (B) Schematic diagram of LUMO and HOMO energy levels of N,S-CDs and CGA.

$$E_{HOMO} = E_{LUMO} - E_g \quad (3)$$

where E_{red} is the potential of reduction peak for N,S-CDs, and E_g the band gap. Based on the Tauc plot (Fig. S3), the E_g was calculated to be 3.99 eV. Then, the E_{HOMO} was estimated to be −7.15 eV from equation (3). As shown in Fig. 9B, apparently, it is impossible for the electron in the LUMO of N,S-CDs to transfer to the LUMO of CGA molecule, namely electron transfer from N,S-CDs to CGA did not take place. Since the other two reasons are excluded, the fluorescence reduction of N,S-CDs caused by CGA is mainly due to IFE process.

3.6. Detection of CGA in real samples

In order to verify the accuracy and feasibility of the ratiometric fluorescent platform for detecting CGA in real samples, standard addition experiments were performed with shuanghuanglian oral liquid and one human serum samples spiked with different amounts of target under the above optimal conditions. As summarized in Table 2, the RSD is lower than 0.8% and the spike recoveries are in the range of 95.4–105.1%, indicating that the sensing system has good reliability in the detection of CGA in real samples.

4. Conclusion

In this paper, one novel highly fluorescent nitrogen and sulfur co-doped carbon dots were successfully via hydrothermal treatment. The obtained N,S-CDs can emit more strong blue fluorescence under UV irradiation due to PEI passivation. Interestingly, the aggregated N,S-CDs have two distinct fluorescence excitation bands corresponding to the same maximum emission wavelength. Based on this phenomenon, a dual-excitation ratiometric fluorescence sensor was developed for the detection of CGA. The proposed sensing platform as an alternative method towards CGA exhibits high sensitivity, better selectivity and stability, meanwhile, it is also an economical, simple and fast detection method. Significantly, by adjusting the excitation peak positions of aggregated N,S-CDs solution, also it can be used to detect other targets using the IFE-based dual-excitation ratiometric fluorescence measurement. This work opens one a new avenue for the application of carbon dots.

Credit author statement

Qingshi Liu, Zhichen Dong and Aijun Hao prepared the samples and performed measurements and data analysis. The final manuscript has been written by Qingshi Liu and Xingjia Guo. Wei Dong and Xingjia Guo discussed the results and commented on the manuscript.

Table 2
Recoveries of CGA in oral liquid and human serum samples using the proposed sensor.

sample	Spiked (μg/mL)	Found[a] (μg/mL)	Recovery (%)	RSD (n = 3) (%)
Oral liquid	0	0.46	–	0.56
	3.33	3.64	95.4	0.73
	6.67	7.08	99.3	0.25
	9.99	10.28	98.3	0.38
Human serum	–	N.D.[b]	–	–
	3.33	3.22	96.7	0.73
	6.67	6.52	97.7	0.63
	9.99	10.50	105.1	0.56

[a] average of three replicate measurements.
[b] N.D. not detected.

Declaration of competing interest

The authors declare that they have no known competing financial interests or personal relationships that could have appeared to influence the work reported in this paper.

Acknowledgments

This project was supported by the Natural Science Foundation of Liaoning Province (No. 20180550105) and the Research Foundation of Shenyang Medical College (No.20139703.20151004). The authors also thank their colleagues and other students who participated in this work.

Appendix A. Supplementary data

Supplementary data to this article can be found online at https://doi.org/10.1016/j.talanta.2020.121372.

References

[1] X. Xu, R. Ray, Y. Gu, H.J. Ploehn, L. Gearheart, K. Raker, W.A. Scrivens, Electrophoretic analysis and purification of fluorescent single-walled carbon nanotube fragments, J. Chem. Soc. 126 (40) (2004) 12736–12737.
[2] S.Y. Lim, W. Shen, Z.Q. Gao, Carbon quantum dots and their applications, Chem. Soc. Rev. 44 (1) (2015) 362–381.
[3] H.T. Li, Z.H. Kang, Y. Liu, S.T. Lee, Carbon nanodots: synthesis, properties and applications, J. Mater. Chem. 22 (46) (2012) 24230–24253.
[4] D.Y. Pan, J.C. Zhang, Z. Li, M.H. Wu, Hydrothermal route for cutting graphene sheets into blue-luminescent graphene quantum dots, Adv. Mater. 22 (6) (2010) 734–739.
[5] X.T. Zheng, A. Ananthanarayanan, K.Q. Luo, P. Chen, Glowing graphene quantum dots and carbon dots: properties, syntheses, and biological applications, Small 11 (14) (2015) 1620–1636.
[6] Y.F. Wang, A.G. Hu, Carbon quantum dots: synthesis, properties and applications, J. Mater. Chem. 2 (34) (2014) 6921–6939.

[7] T. Pal, S. Mothiyuddin, G. Packirisamy, Facile and green synthesis of multicolor fluorescence carbon dots from curcumin: in vitro and in vivo bioimaging and other applications, ACS Omega 3 (1) (2018) 831–843.
[8] T. Pal, S. Mothiyuddin, G. Packirisamy, Facile and green synthesis of multicolor fluorescence carbon dots from curcumin: in vitro and in vivo bioimaging and other applications, ACS Omega 3 (5) (2018), 5887-5887.
[9] M.H. Xu, S.S. Xu, Z. Yang, M.J. Shu, G.L. He, D. Huang, L.L. Zhang, L. Li, D.X. Cui, Y.F. Zhang, Hydrophilic and blue fluorescent N-doped carbon dots from tartaric acid and various alkylol amines under microwave irradiation, Nanoscale 7 (38) (2015) 15915–15923.
[10] Z.S. Qian, X.Y. Shan, L.J. Chai, J.J. Ma, J.R. Chen, H. Feng, Si-doped darbon quantum dots: a facile and general preparation strategy, bioimaging application, and multifunctional sensor, ACS Appl. Mater. Interfaces 6 (9) (2014) 6797–6805.
[11] X.A. Miao, X.L. Yan, D. Qu, D.B. Li, F.F. Tao, Z.C. Sun, Red emissive sulfur, nitrogen codoped carbon dots and their application in ion detection and theraonostics, ACS Appl. Mater. Interfaces 9 (22) (2017) 18549–18556.
[12] H. Ding, J.S. Wei, H.M. Xiong, Nitrogen and sulfur co-doped carbon dots with strong blue luminescence, Nanoscale 6 (2015) 13817–13823.
[13] W. Dong, S.Q. Zhou, Y. Dong, J.W. Wang, X. Ge, L.L. Sui, The preparation of ethylenediamine-modified fluorescent carbon dots and their use in imaging of cells, Luminescence 30 (6) (2015) 867–871.
[14] B.F. Han, W.X. Wang, H.Y. Wu, F. Fang, N.Z. Wang, X.J. Zhang, S.K. Xu, Polyethyleneimine modified fluorescent carbon dots and their application in cell labeling, Colloids Surf., B 100 (2012) 209–214.
[15] C.J. Liu, P. Zhang, X.Y. Zhai, F. Tian, W.C. Li, J.H. Yang, Y. Liu, H.B. Wang, W. Wang, W.G. Liu, Nano-carrier for gene delivery and bioimaging based on carbon dots with PEI-passivation enhanced fluorescence, Biomaterials 33 (13) (2012) 3604–3613.
[16] X.H. Gu, R. Xu, G.L. Yuan, H. Lu, B.R. Gu, H.P. Xie, Preparation of chlorogenic acid surface-imprinted magnetic nanoparticles and their usage in separation of traditional Chinese medicine, Anal. Chim. Acta 675 (1) (2010) 64–70.
[17] W.Y. Huang, Y.Z. Cai, Y.B. Zhang, Natural phenolic compounds from medicinal herbs and dietary plants: potential use for cancer prevention, Nutr. Canc. 62 (1) (2010) 1–20.
[18] Y. Sato, S. Itagaki, T. Kurokawa, J. Ogura, M. Kobayashi, T. Hirano, M. Sugawara, K. Iseki, In vitro and in vivo antioxidant properties of chlorogenic acid and caffeic acid, Int. J. Pharm. 403 (1–2) (2011) 136–138.
[19] H. Hemmerle, H.J. Burger, P. Below, G. Schubert, R. Rippel, P.W. Schindler, E. Paulus, A.W. Herling, Chlorogenic acid and synthetic chlorogenic acid derivatives: novel inhibitors of hepatic glucose-6-phosphate translocase, J. Med. Chem. 40 (2) (1997) 137–145.
[20] V. Nour, I. Trandafir, S. Cosmulescu, HPLC determination of phenolic acids, flavonoids and juglone in walnut leaves, J. Chromatogr. Sci. 51 (9) (2013) 883–890.
[21] R. Jaiswal, H. Muller, A. Muller, M.G.E. Karar, N. Kuhnert, Identification and characterization of chlorogenic acids, chlorogenic acid glycosides and flavonoids from Lonicera henryi L. (Caprifoliaceae) leaves by LC-MS, Phytochemistry 108 (2014) 252–263.
[22] R. Jaiswal, N. Kuhnert, How to identify and discriminate between the methyl quinates of chlorogenic acids by liquid chromatography-tandem mass spectrometry, J. Mass Spectrom. 46 (3) (2011) 269–281.
[23] V. Lebot, S. Michalet, L. Legendre, Identification and quantification of phenolic compounds responsible for the antioxidant activity of sweet potatoes with different flesh colours using high performance thin layer chromatography (HPTLC), J. Food Compos. Anal. 49 (2016) 94–101.
[24] X.D. Wang, P.F. Yin, H.P. Gong, P.P. Li, Z.Q. Liu, Y.Q. He, Reversible fluorescence regulation based on water-soluble CdTe quantum dot-chlorogenic acid-angiotensin I interaction, Chem. J. Chin. Univ. 33 (6) (2012) 1182–1187.
[25] H. Yang, L. Yang, Y.S. Yuan, S. Pan, J.D. Yang, J.J. Yan, H. Zhang, Q.Q. Sun, X. L. Hu, A portable synthesis of water-soluble carbon dots for highly sensitive and selective detection of chlorogenic acid based on inner filter effect, Acta Part A 189 (2018) 139–146.
[26] F.Y. Yan, Z.J. Bai, T.C. Ma, X.D. Sun, F.L. Zu, Y.M. Luo, L. Chen, Surface modification of carbon quantum dots by fluorescein derivative for dual-emission ratiometric fluorescent hypochlorite biosensing and in vivo bioimaging, Sensor. Actuator. B Chem. 296 (2019) 126638–126646.
[27] Z.C. Xu, K.H. Baek, H.N. Kim, J.N. Cui, X.H. Qian, D.R. Spring, I. Shin, J. Yoon, Zn^{2+}-triggered amide tautomerization produces a highly Zn^{2+}-selective, cell-permeable, and ratiometric fluorescent sensor, J. Am. Chem. Soc. 132 (2) (2010) 601–610.
[28] J.Y. Chen, M.K. Wang, X.G. Su, Ratiometric fluorescent detection of azodicarbonamide based on silicon nanoparticles and quantum dots, Sensor. Actuator. B Chem. (2019) 296.
[29] H.Y. Xu, K.N. Zhang, Q.S. Liu, Y. Liu, M.X. Xie, The visual and fluorescent detection of mercury ions by using a dually emissive ratiometric nanohybrid containing carbon dots and CdTe quantum dots, Microchim Acta 184 (4) (2017) 1196–1206.
[30] X.H. Li, X.H. Gao, W. Shi, H.M. Ma, Design strategies for water-soluble small molecular chromogenic and fluorogenic probes, Chem. Rev. 114 (1) (2014) 590–659.
[31] X.L. Zhang, Y. Xiao, X.H. Qian, A ratiometric fluorescent probe based on FRET for imaging Hg^{2+} ions in living cells, Angew. Chem. Int. Ed. 47 (42) (2008) 8025–8029.
[32] K.M. Omer, D.I. Tofiq, D.D. Ghafoor, Highly photoluminescent label free probe for Chromium (II) ions using carbon quantum dots co-doped with nitrogen and phosphorous, J. Lumin. 206 (2019) 540–546.
[33] P.C. Hsu, H.T. Chang, Synthesis of high-quality carbon nanodots from hydrophilic compounds: role of functional groups, Chem. Commun. 48 (33) (2012) 3984–3986.
[34] X.A. Miao, X.L. Yan, D. Qu, D.B. Li, F.F. Tao, Z.C. Sun, Red emissive sulfur, nitrogen codoped carbon dots and their application in ion detection and theraonostics, ACS Appl. Mater. Interfaces 9 (22) (2017) 18549–18556.
[35] J.X. Duan, J. Yu, S.L. Feng, L. Su, A rapid microwave synthesis of nitrogen-sulfur co-doped carbon nanodots as highly sensitive and selective fluorescence probes for ascorbic acid, Talanta 153 (2016) 332–339.
[36] Y.Q. Dong, H.C. Pang, H.B. Yang, C.X. Guo, J.W. Shao, Y.W. Chi, C.M. Li, T. Yu, Carbon-based dots co-doped with nitrogen and sulfur for high quantum yield and excitation-independent emission, Angew. Chem. Int. Ed. 52 (33) (2013) 7800–7804.
[37] J. Shen, T. Zhang, Y. Cai, X.Y. Chen, S.M. Shang, J. Li, Highly fluorescent N,S-co-doped carbon dots: synthesis and multiple applications, New J. Chem. 41 (19) (2017) 11125–11137.
[38] Y.F. Chen, Y.Y. Wu, B. Weng, B. Wang, C.M. Li, Facile synthesis of nitrogen and sulfur co-doped carbon dots and application for Fe(III) ions detection and cell imaging, Sensor. Actuator. B Chem. 233 (2016) 689–696.
[39] X. Fang, X.Q. Li, H. Wang, X.M. Wu, G.L. Wang, Tuning surface states to achieve the modulated fluorescence of carbon dots for probing the activity of alkaline phosphatase and immunoassay of alpha-fetoprotein, Sensor. Actuator. B Chem. 257 (2018) 620–628.
[40] N. Grujic, Z. Lepojevic, B. Srdjenovic, J. Vladic, J. Sudji, Effects of different extraction methods and conditions on the phenolic composition of mate tea extracts, Molecules 17 (2012) 2518–2528.
[41] K.A.P. Sousa, F.M.R. Lima, T.O. Monteiro, S.M. Silva, M.O.F. Goulart, F.S. Damos, R.D.S. Luz, Amperometric photosensor based on acridine orange/TiO_2 for chlorogenic acid determination in food samples, Food Anal. Method. 11 (10) (2018) 2731–2741.
[42] I. Tomac, M. Seruga, E. Beinrohr, Characterization of chlorogenic acids in coffee by flow-through chronopotentiometry, Food Anal. Method. 10 (12) (2017) 3924–3933.
[43] E.A. Dil, A. Asfaram, F. Sadeghfar, Magnetic dispersive micro-solid phase extraction with the CuO/ZnO@Fe_3O_4-CNTs nanocomposite sorbent for the rapid pre-concentration of chlorogenic acid in the medical extract of plants, food, and water samples, Analyst 144 (8) (2019) 2684–2695.
[44] F. Zu, F. Yan, Z. Bai, J. Xu, Y. Wang, Y. Huang, X. Zhou, The quenching of the fluorescence of carbon dots: a review on mechanisms and applications, Microchim Acta 184 (2017) 1899–1914.